THE DEVELOPMENT OF A MINIATURIZED HEATER FOR THIN FILM OXYGEN PARTIAL PRESSURE SENSORS

A Thesis

Presented to

the Faculty of the School of Engineering and Applied Science

University of Virginia

In Partial Fulfillment

of the Requirements for the Degree

Master of Electrical Engineering

---

by

Carl Raymond Pearson

August 1969

APPROVAL SHEET

This thesis is submitted in partial fulfillment of

the requirements for the degree of

Master of Electrical Engineering

Author

Approved:

Faculty Adviser

Dean, School of Engineering
and Applied Science

August 1969

ABSTRACT

The feasibility of using a miniature heater for a zinc oxide thin film oxygen partial pressure sensor was investigated. A silicon heater 0.010 inch square by 1/2 inch long was used to obtain a 400° C surface temperature. The temperature of the heater can be measured by the change in resistance of the heater at its operating temperature. Experimental data are presented for the resistance-temperature characteristics, the temperature distribution, and power requirements of the heater. This work has shown that this heater concept is feasible, but more effort will be required to deposit the zinc oxide film on the heater surface.

ACKNOWLEDGMENTS

The author wishes to acknowledge Dr. E. C. Stevenson of the University of Virginia, Dr. J. J. Wortman and Mr. T. M. Royal of Research Triangle Institute for their helpful suggestions in the preparation of this thesis, plus the NASA Langley Research Center for making it possible for this work to be submitted as a thesis.

TABLE OF CONTENTS

LIST OF FIGURES

LIST OF SYMBOLS

A	cross-sectional area
A_s	surface area
A_o	constant
B	area of electrical contact
c	electron charge
C	constant
D	cross-sectional dimension of heater
E_c	energy of condition band edge
E_f	Fermi energy level
E_g	width of the forbidden energy gap
E_m	metal work function
E_s	semiconductor work function
E_v	energy of valence band edge
E_w	height of potential barrier
$\mathcal{E}$	electric field intensity
F_T	temperature factor
h_c	convective heat-transfer film coefficient
h_r	radiant heat-transfer film coefficient
I	current
$I_{m \rightarrow s}$	current flowing from metal to semiconductor
$I_{s \rightarrow m}$	current flowing from semiconductor to metal
J	current density
k	Boltzmann's constant
K	constant

K'	constant
n	electron density
N_c	effective density of states in conduction band
N_v	effective density of states in valence band
p	hole density
q	rate of heat flow
R	resistance
T	temperature
T_o	ambient temperature
V	voltage
x	distance
α	emissivity
σ	conductivity
ϵ	permittivity
μ_e	electron mobility
μ_h	hole mobility
ρ	resistivity

CHAPTER I

INTRODUCTION

All of our past space flights have been flown with a nearly 100 per cent oxygen atmosphere. This atmosphere was selected for the Mercury flights because it allowed the atmospheric supply and control system to have the lowest possible weight. The small thrust capabilities of the first manned launch vehicles made this a very important decision.

I. The Need for Oxygen Sensing

As the length of the space mission is extended, physiological and fire hazard considerations become more important than the weight savings of a nearly 100 per cent oxygen atmosphere. There are a number of conflicting problems in selecting a cabin atmosphere. The cabin pressure should be an absolute minimum to reduce the pressure difference across the pressure hull. This would allow the pressure hull to have the minimum possible weight. For the health of the astronauts in a long-term mission, the total pressure and oxygen partial pressure must be within certain limits. Also, the fire hazard is increased as the oxygen partial pressure is increased.

The atmosphere selected for the Advanced Apollo Applications and Manned Orbiting Laboratory programs consists of a 5 psia total pressure with about 65 per cent oxygen. AAP uses a nitrogen diluent and MOL uses a helium diluent.

Current extravehicular activity and lunar excursion space suits use a pure oxygen environment at 3 psia. This atmosphere was selected

mainly because mobility of current suits is greatly reduced at higher pressures. Once this problem is eliminated, all current indications point toward the use of a reduced oxygen atmosphere for this application also.

Any atmosphere other than 100 per cent oxygen requires an oxygen sensor in order to measure and control the required level of oxygen.

II. Problems in Sensing Oxygen

When the requirements of space flight are applied to the possible methods of accurately sensing oxygen partial pressure, a very limited number of currently known methods remain feasible. The sensing and control system must have low weight, small size, and small power consumption plus the ability to operate in a zero gravity condition and withstand the vibration and acceleration loads of flight. In addition, the sensor must have an electrical signal output that is specific only to oxygen with at least a 2 to 5 per cent accuracy and stability over a 100-day period.

These requirements rule out most of the standard chemical analysis techniques that might at first be considered and leave techniques based more on the physical and electrical properties of oxygen.

III. Available Sensing Techniques

The best commercially available laboratory standard oxygen sensor makes use of the paramagnetic properties of oxygen. Not only is oxygen strongly paramagnetic, but also, no other gas with paramagnetic or diamagnetic properties is present in sufficient quantities to influence the sensor output. This technique would be perfect for spacecraft applications except that the magnetic forces involved are so small that a

delicate measuring setup is required to detect them. A delicate instrument cannot pass the vibration and acceleration specifications for launch.

The polarographic oxygen sensor makes use of an electrochemical reaction to produce an output proportional to the oxygen partial pressure. While this sensor meets most of the flight requirements, it is subject to considerable output drift over long time periods.

Oxygen has a usable absorption frequency in the ultraviolet range. A considerable amount of effort has been expended to design a flight sensor using this technique, but no workable device has been produced.

Another sensor, termed a solid electrolyte sensor, makes use of a technique involving the conduction of ionic oxygen through a ceramic crystal lattice. A differential voltage is produced that is proportional to the ratio of the oxygen partial pressures on the two sides of the ceramic. In order to achieve reasonable stability and freedom from poisoning, this sensor must be operated at 850° Centigrade. Although a commercial sensor using this technique is available, efforts to miniaturize the sensor and reduce its electrical power requirements have led to many problems achieving hermetic seals at the 850° operating temperature.

A very successful sensor, which is capable of being flight qualified, has been developed using a magnetic sector mass spectroscopy technique. This sensor measures oxygen, nitrogen, carbon dioxide, and water vapor partial pressures. It weighs approximately 5 pounds and requires about 5 watts of power. This sensor is very well suited for sensing a spacecraft atmosphere, but other applications, such as future lunar

excursion and extravehicular activity space suits, will require an oxygen sensor that is considerably lighter and less demanding of power.

The sensor which seems to have the greatest promise in being able to successfully meet all requirements is the zinc oxide thin film oxygen sensor.

IV. Zinc Oxide Thin Film Oxygen Partial Pressure Sensor

Zinc oxide has been used for many years as a pigment for paint, as an activator for the vulcanization of rubber, and as a catalyst and photocatalyst for chemical reactions (Ref. 1, p. 193). A considerable amount of research has been done on this material in the last 30 years. In 1950, Bevan and Anderson (Ref. 2) reported data on the variation of electrical conductance of zinc oxide with oxygen pressure at different temperatures. Kefeli in 1957 (Ref. 3) proposed using this effect to measure oxygen.

Under Contract NAS1-7087, Research Triangle Institute conducted an investigation of zinc oxide thin film for sensing oxygen and constructed a laboratory model using this technique (Ref. 4). Their working model consisted of a nichrome wire heating element surrounded by a hollow cylindrical substrate on which a zinc film was deposited and then oxidized at 600° C. This whole unit was then enclosed in an insulating housing similar to a miniature thermos bottle. This arrangement resulted in a sensor weighing about 30 grams, occupying approximately 30 cubic centimeters of volume and requiring 5 to 6 watts of power for operation at 400° C.

In general, the zinc oxide operates as a doped semiconductor. A number of different models can each be used to describe the properties of zinc oxide under different conditions. If the oxygen is considered to diffuse into the bulk material or be adsorbed on the surface, the end result is to form new acceptor sites and thus reduce the density of conduction electrons in the n-type film. Since the conductivity is proportional to the electron density, the conductivity is inversely proportional to the oxygen partial pressure. A much more detailed treatment of the theoretical operation of zinc oxide thin films is given by Royal, Wortman, and Monteith (Ref. 4, pp. 17-30).

The electrical conductivity and the time required to respond to a change in oxygen partial pressure are both temperature dependent. The response time decreases with increasing temperature. The temperature dependence of the electrical conductivity is shown in Figure 1. The minimum in the curve at 400° C is the best operating point for this technique for two reasons. First, the time required for the sensor output to respond to 50 per cent of its final value for a change from pure oxygen to pure nitrogen atmosphere varies from 30 seconds to 6 minutes at this temperature, depending on the direction of the change. Secondly, the slope of the conductance versus temperature curve at this point is small. As can be seen in Figure 1, 60° and 100° temperature changes result in only 1 and 5 per cent changes, respectively, in electrical conductance. This relatively weak dependence upon temperature at this point minimizes the required temperature control accuracy and the effect of a temperature gradient along the required heater (Ref. 4, pp. 43-44).

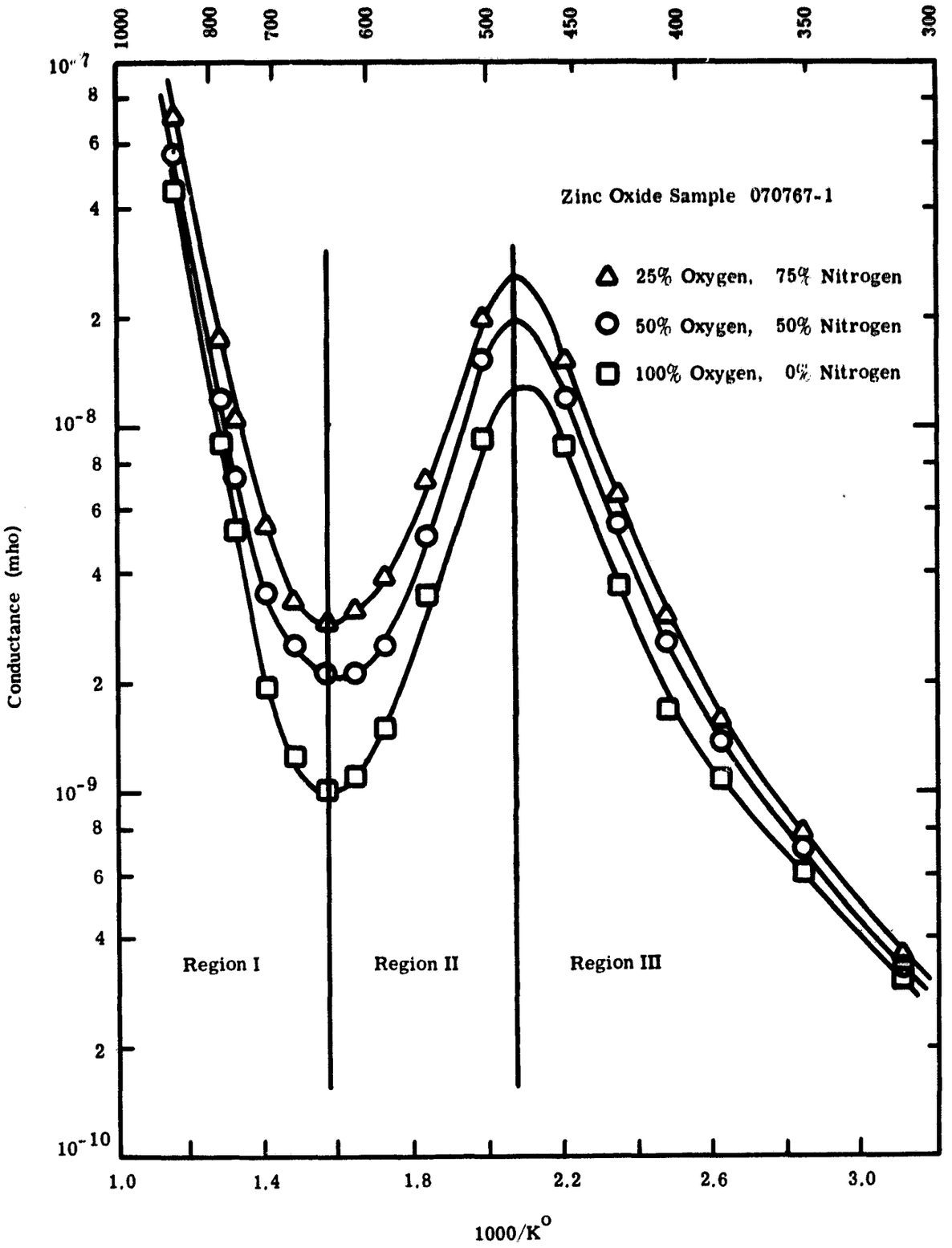

Figure 1.- Electrical conductance of zinc oxide vs increasing temperature for various partial pressures of oxygen. (Ref. 4, p. 5)

V. Concept of Miniaturized Heater for Thin Film Sensor

In any design of a high-temperature heater, the required heater input power is inversely proportional to the amount of insulation present and proportional to the surface area of the heater. Minimizing the surface area will minimize the convective and radiant heat losses.

The convective heat loss is given by

$$q_c = A_s h_c (T - T_o) \tag{1}$$

where

A_s = surface area

h_c = film coefficient

T = surface temperature in ^oK

T_o = surrounding air temperature in ^oK

The radiant heat loss is given by

$$q_r = A_s h_r (T - T_o) \tag{2}$$

where

$$h_r = \alpha F_t$$

$$F_t = \frac{1.81\left[\left(\frac{T}{100}\right)^4 - \left(\frac{T_o}{100}\right)^4\right]}{T - T_o}$$

α = emissivity (Ref. 5, pp. 331,202-211)

In decreasing the cross-sectional dimensions of the heater in order to decrease the surface area, two problems become evident. The heater material will have to be selected so that it will not require excessive driving voltage or current. High voltages or large currents could only be provided by a special converter whose weight and volume would be charged to the sensor. Also, small size aggravates the problems of electrical connections and heater temperature sensing.

The objectives of this work were as follows:

1. Minimize heater power by making dimensions as small as practical.
2. Select a heater material with proper resistivity.
3. Develop reliable electrical connections to the heater.
4. Develop a method of measuring the heater temperature.

CHAPTER II

SELECTION OF HEATER MATERIAL

I. Approximate Range of Resistivity

The following parameters were chosen as the initial design criteria for a heater consisting of a single short length of conductor: (1) voltage less than 100 volts, (2) current between 1 and 100 milliamperes, (3) resistance between 500 and 5,000 ohms, (4) length of the heater between 1/4 and 1/2 inch, and (5) heater diameter between 0.001 and 0.050 of an inch.

Using these values, the maximum acceptable resistivity is 100 ohm-centimeters and the minimum is 0.002 ohm-centimeters at 400° C, a range falling within the properties of semiconducting materials. Since silicon is probably the most readily available and most highly documented semiconducting material, it was selected for the heater.

II. Silicon Heater

Since the resistivity of any semiconductor is a function of its doping level in the extrinsic region, the resistivity can be adjusted to achieve the desired miniature sized heater.

The effect of temperature on the resistivity of silicon for various doping levels is shown in Figure 2. Silicon has a positive temperature coefficient of resistivity in its extrinsic range. In the intrinsic region the temperature coefficient of resistivity is negative and the logarithm of the resistivity is directly proportional to the reciprocal of the temperature.

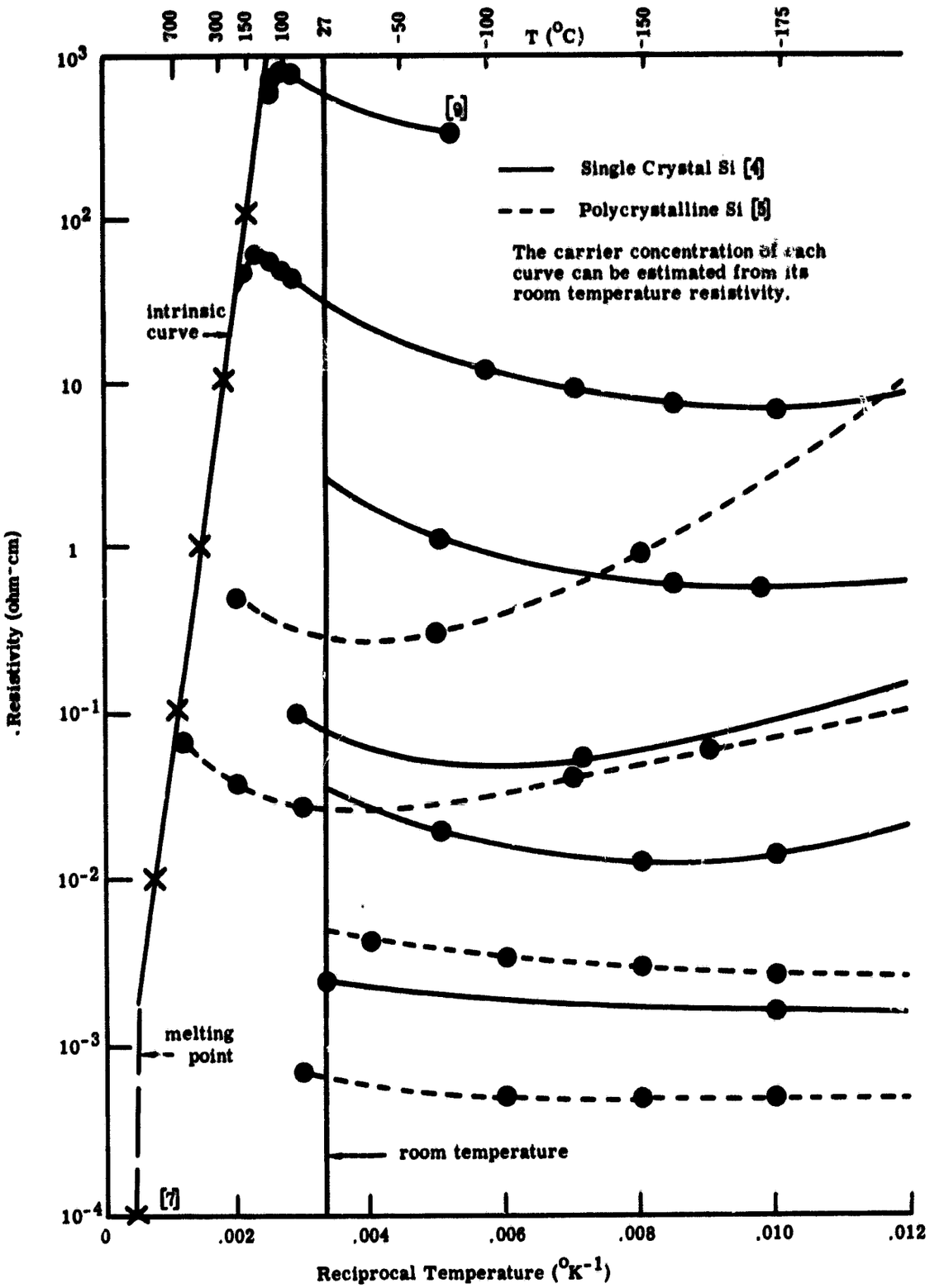

Figure 2.- The temperature dependence of resistivity for n-type silicon. (Ref. 6, p. 22)

The room temperature resistivity of silicon can be selected so that at 400° C the silicon bar is operating in its intrinsic region. A cross-sectional dimension of 0.010 inch was selected to simplify fabrication problems.

In order to make use of the constant temperature coefficient of log resistance for the intrinsic region to sense the temperature, as discussed in Chapter IV, a room temperature resistivity of approximately 1 ohm-centimeter was chosen. With a heater length of 1/2 inch, and assuming the whole bar to be at 400° C, the heater resistance should be approximately 2,500 ohms.

A silicon bar with a room temperature resistivity of 0.8 ohm-centimeter and the following dimensions was procured.

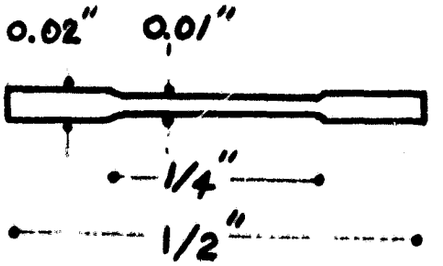

CHAPTER III

HEATER ELECTRICAL CONTACTS

I. Achieving Electrical Contact

Gold wires 0.001 inch in diameter were first used in an attempt to make electrical connections to the bar. They were thermocompression bonded to an aluminum pad deposited on the bar ends. This is a standard technique used in microelectronic circuitry, and the contacts were expected to be capable of carrying the necessary current. However, the wires melted just before the thermocompression bond bead at a current of 11 milliamperes. An attempt to parallel three 0.001-inch gold wires was also unsuccessful; all three melted at a current of 18.7 milliamperes.

Liquid bright gold paste leads fired on the bar proved to be a successful method of achieving electrical contacts. The gold paste was painted on the ends of the bar, down the ceramic supports, and on to conducting pads on the base.

Liquid bright gold contacts have been known to degrade in a few days when operated at elevated temperatures (Ref. 4, p. 3). In this particular application no degradation has been noticed over periods as long as 6 months. The ends of the bar where the contacts are located are not at a temperature anywhere near 400° C. This is the most likely reason for the stability.

Although the electrical contact problem was solved, the bar resistance was found to be a function of the current for currents small enough to cause no measurable temperature rise.

II. Ohmic Contact Problems

When a junction is formed between a metal and a semiconductor, either one of two types of contacts are formed.

If the work function of the metal is greater than the work function of the n-type semiconductor, electrons flow from the semiconductor to the metal when contact is made. This flow continues until a negative charge is built up and the Fermi levels are continuous across the junction. This forms a potential barrier at the junction which can be increased or decreased by applying an external potential of the proper polarity. The magnitude of the net current flow is inversely proportional to the barrier potential which is influenced by the polarity of the applied voltage. Thus a rectifying junction is formed.

If the work function of the metal is less than the work function of the n-type semiconductor, electrons flow from the metal to the semiconductor. This results in the lack of any potential barrier at the junction. The magnitude of the net current flow is independent of the polarity of the applied voltage. This is characteristic of an ohmic contact between the metal and semiconductor.

In actual practice the height of the potential barrier is more dependent on the surface states of the semiconductor than on the metal work function. If the surface state density is large enough, contact with the metal causes electron flow between the metal and the surface states instead of the bulk material. If the surface states are not removed, a rectifying contact will be formed (Ref. 7, pp. 227-233).

When electrical contact is made to each end of a semiconducting material with rectifying contacts, one or the other of the two rectifying contacts will be reverse biased for either polarity of applied voltage.

The current flowing in each direction across a metal semiconductor junction is dependent on the thermionic emission of electrons across a potential barrier. This current is given by the Richardson-Dushman equation

$$J = A_o T^2 \, e^{-E_w/kT} \tag{3}$$

where

J = current density

$A_o = 1.2 \times 10^6$ amps/m^2-^oK

T = temperature

E_w = height of potential barrier

k = Boltzmann's constant (Ref. 7, pp. 232,313)

When an electric field is applied, the thermionic emission is influenced by the space charge of the emitted electrons. This is called Schottky effect and is given by

$$J = A_o T^2 \, e^{-\left[E_w - c(c\mathcal{E}/4\pi\epsilon)^{1/2}\right]/kT} \tag{4}$$

where

c = electron charge

$\mathcal{E}$ = electric field

ϵ = permittivity (Ref. 7, p. 317)

In a rectifying contact, the current from the metal has to overcome a potential barrier equal to the difference between the metal and the semiconductor work functions. This current is then

$$I_{m\to s} = BA_oT^2\, e^{-\left[E_m - E_s - K\mathcal{E}^{1/2}\right]/kT} \qquad (5)$$

where

B = area of the contact

E_m = metal work function

E_s = semiconductor work function

$$K = c\left(\frac{c}{4\pi\epsilon}\right)^{1/2}$$

The current from the semiconductor has to overcome the barrier equal to $E_m - E_s - cV$, where V is the applied voltage. V is positive for forward bias and negative for reverse bias. This current is then

$$I_{s\to m} = BA_oT^2\, e^{-\left[E_m - E_s - K\mathcal{E}^{1/2} - cV\right]/kT} \qquad (6)$$

The net current is then

$$I = I_{s\to m} - I_{m\to s}$$

Since one of the contacts will always be reverse biased, it will limit the current for the whole bar. For this situation, the forward current $I_{s\to m}$ will be negligible compared to the reverse current. The net current will be

$$I = BA_o T^2 \, e^{-\left[E_m - E_s - K\mathcal{E}^{1/2}\right]/kT}$$

$$\ln I = \ln\left[BA_o T^2\right] - \frac{(E_m - E_s)}{kT} + \frac{K}{kT}\mathcal{E}^{1/2}$$

Assume

$$C = \ln\left[BA_o T^2\right] - \left[\frac{E_m - E_s}{kT}\right]$$

$$K' = \frac{K}{kT}$$

Then

$$\ln I = K'\mathcal{E}^{1/2} + C \qquad (7)$$

The characteristics of the contacts for the 0.01-inch silicon bar with fired-on liquid bright gold contacts is shown in Figure 3. This is a plot of the bar current as a function of the square root of the voltage applied to the bar for currents sufficiently small so as not to cause any measurable rise in the bar temperature. For these low currents, the voltage drop across the bar can be neglected compared to the drop across the reverse biased rectifying contact. If it is assumed that $\mathcal{E} = V/x$, where x is the width of the space charge region, equation (7) would then become

$$\ln I = K'x^{-1/2}V^{1/2} + C \qquad (8)$$

Although both curves in Figure 3 have straight line segments, the slope of the lines increases at 1.5 to 2.0 volts$^{1/2}$. This could be

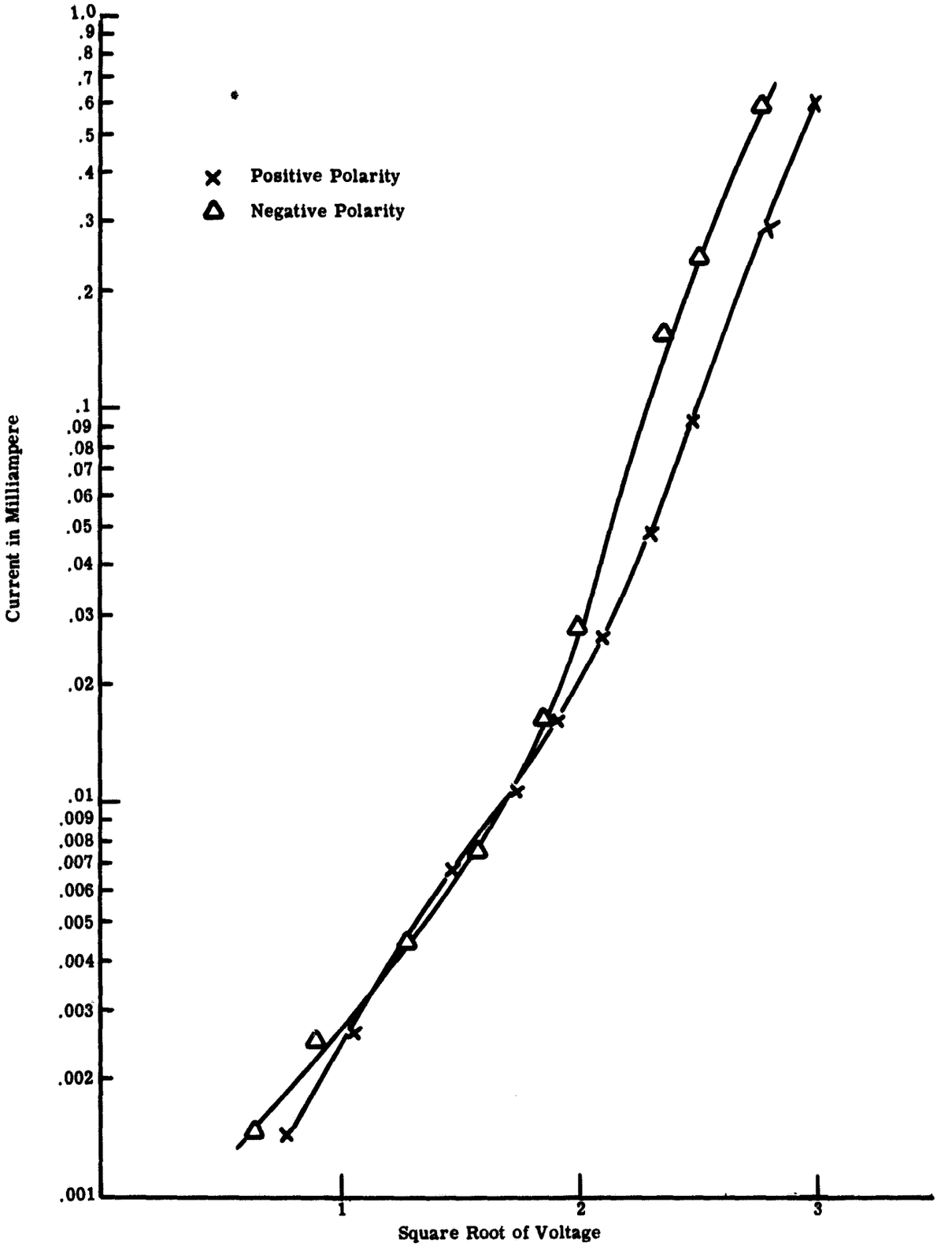

Figure 3.- Current as a function of square root of applied voltage for both polarities.

accounted for by a decrease in the space charge width as the voltage is increased.

These data are sufficiently close to the characteristics of a rectifying contact to verify that the contacts are responsible for this effect.

As the current and therefore the bar temperature increase, the rectifying contact will break down to the point where it has a negligible effect on the bar resistance. At the 400° operating temperature, the resistance characteristics will be due to the silicon bar alone.

CHAPTER IV

MEASUREMENT OF HEATER TEMPERATURE

The temperature of a heater as small as 0.01 inch is very hard to measure by conventional means without establishing an undesirably large heat drain.

I. Change in Resistance of Heater to Sense Heater Temperature

As shown in Figure 1, page 6, the logarithm of the resistivity of silicon is a linear function of inverse temperature for the intrinsic region. Figure 4 shows the resistivity of silicon plotted against temperature instead of inverse temperature. The change in the slope of the intrinsic curve from about 350 to 450° C is small. Thus, over this limited range the logarithm of the resistivity can be assumed to be linearly dependent on temperature and the logarithm of the conductivity will be directly proportional to temperature.

Thus a signal proportional to the temperature of the heater in the intrinsic region can be obtained by dividing a signal proportional to the heater current by a signal proportional to the heater voltage. A standard analog computational device is commercially available whose output is proportional to the logarithm of the ratio between two input signals.

Once the resistance-temperature characteristics of the heater are known, this latter method would allow the heater temperature to be measured completely external to the heater. Although there will be a

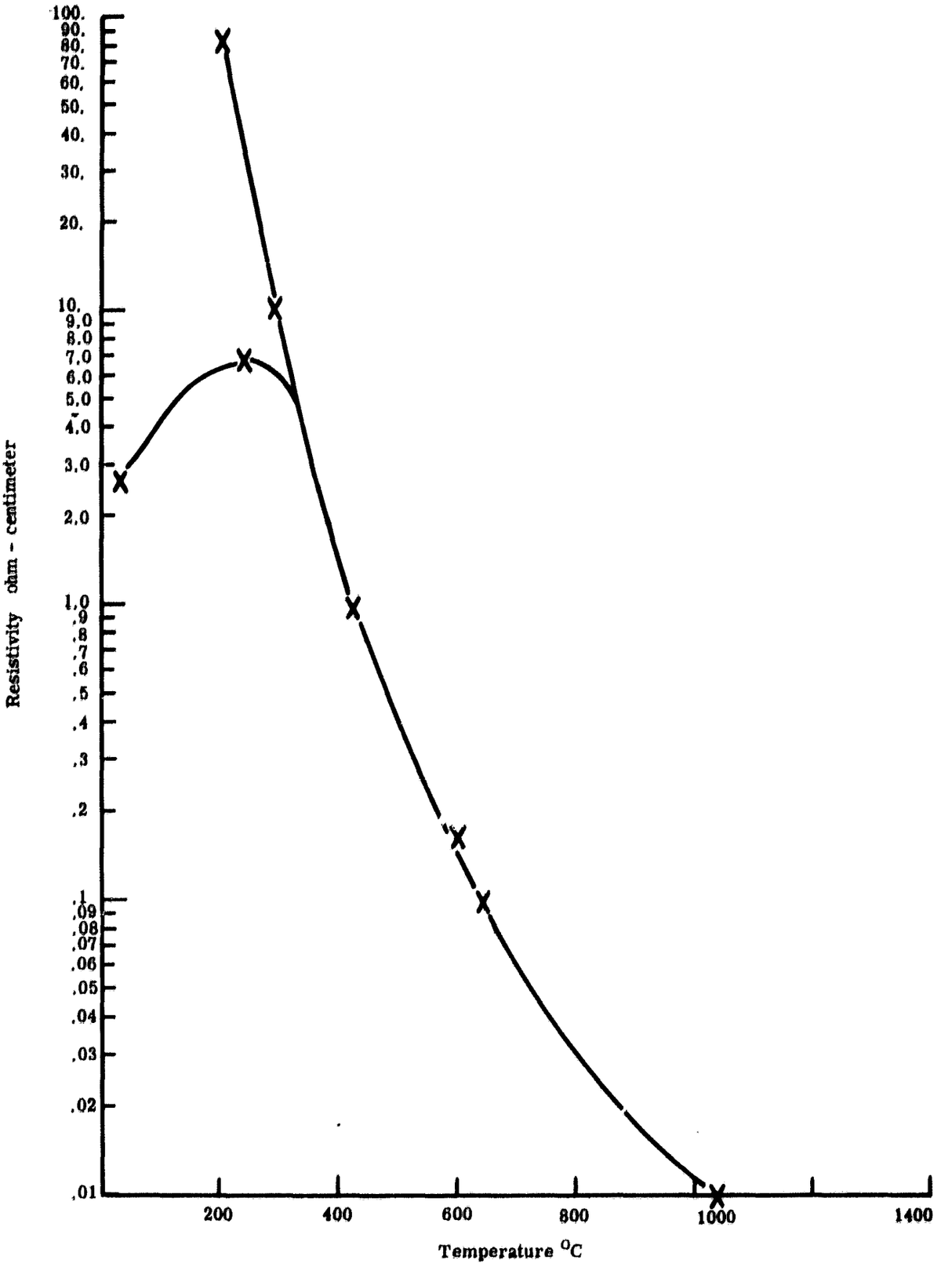

Figure 4.- Resistivity as a function of temperature for silicon.

temperature gradient along the heater, the relative insensitivity of the zinc oxide film to temperature variations at 400° C would minimize this problem. The actual temperature distribution for the heater is discussed in Chapter VI.

II. Practical Experimental Temperature Measurement

Although the heater temperature will be measured in use by the foregoing resistance change method, this method requires a calibration technique for determining the bar resistance-temperature characteristics.

One of the first methods considered for measuring the temperature was the use of an infrared spectrophotometer. A survey of commercially available instruments was made. Although it was possible to focus such an instrument down to 0.010 inch, a temperature of 400° C was below its accurate usable range.

An attempt was made to heat the bar in a furnace and measure its resistance as a function of the furnace air temperature. Due to the rectifying contacts which caused the measured resistance to be a function of the measuring current, this method was discarded as being unreliable. Also, since in operation the whole bar would not be at the same temperature, this method would not give directly applicable results.

The method finally selected consisted of using a commercially available microminiature copper constantan thermocouple junction. This thermocouple consisted of 0.001-inch-diameter wires sheathed in a 0.030-inch-diameter stainless steel tube. The wires protrude beyond the tube and are formed into a junction of 0.010 inch diameter. The thermocouple was rigidly mounted, and the heater bar with its ceramic

holder was mounted on the table of a three-axis micropositioner. With the aid of a 120 power stereo zoom microscope, the thermocouple was placed against the surface of the heater. This was measuring the surface temperature which is the temperature of interest for the zinc oxide film.

This is not an ideal way of measuring the temperature, since the thermocouple is about the same size as the heater. The positioning of the thermocouple was critical since any surface irregularities would influence its readings.

Placing the thermocouple on the bar surface would also conduct a certain amount of heat away from the bar and, thus, lower the surface temperature. This heat conduction appeared to be small enough not to influence the data since no change in the heater voltage or current was noted when the thermocouple was placed on the surface.

CHAPTER V

TEMPERATURE CHARACTERISTICS OF SILICON

The conductivity of a semiconductor is given by

$$\sigma = nc\mu_e + pc\mu_h \tag{9}$$

where

σ = conductivity

n = electron density

c = electronic charge

μ_e = electron mobility

p = hole density

μ_h = hole mobility (Ref. 7, p. 203)

I. Theoretical Discussion of Conductivity Versus Temperature

The n-type silicon bar used for the heater had a room temperature resistivity of approximately 0.8 ohm-centimeter. This requires a doping level of about 7.0×10^{15} impurities/cm^3 (Ref. 6, p. 19).

In the extrinsic region, the electron mobility is an extremely complex function of the impurity concentration and temperature for impurity concentrations as large as 10^{15} impurities/cm^3. Theory cannot satisfactorily predict this dependence (Ref. 6, p. 16). The most reliable source for data in this region is experimental data such as is given in Figure 2, page 10, but actually this consideration is only of

limited importance for the operation of the heater since it will not be used in this region.

In the intrinsic region the electron and hole densities are equal and the Fermi level lies midway between the valence and conduction bands. The electron and hole concentrations are given by

$$n = N_c \, e^{-(E_c - E_f)/kT} \tag{10}$$

$$p = N_v \, e^{-(E_f - E_v)/kT} \tag{11}$$

where

N_c = effective density of states in conduction band

N_v = effective density of states in valence band

E_c = energy of conduction band edge

E_v = energy of valence band edge

E_f = Fermi energy (Ref. 7, pp. 199,200)

Assume

$$E_g = E_c - E_v$$

where

E_g = width of the forbidden energy gap

Since

$$E_f \cong \frac{(E_c + E_v)}{2}$$

Then

$$E_c - E_f = E_f - E_v = \frac{E_g}{2}$$

Since

$$\rho = \frac{1}{\sigma}$$

$$\rho = \left[\frac{1}{N_c\, e(\mu_e + \mu_h)}\right] e^{E_g/2kT}$$

$$\ln \rho = -\ln\left[N_c\, e(\mu_e + \mu_h)\right] + \frac{E_g}{2kT} \qquad (12)$$

The change in the first term with temperature is small compared to the second term, so that a plot of $\ln \rho$ versus $1/T$ will be a straight line of slope $E_g/2k$.

II. Resistance Versus Temperature

Experimental Data

Figure 5 shows the experimentally measured dependence of the logarithm of the resistance of the silicon bar heater on temperature. The 0.010-inch-square by 1/2-inch-long bar was mounted in an alumina frame with fired-on liquid bright gold electrical contacts. A variable constant current power supply was used to supply power to the heater. The temperature was measured by a microminiature copper constantan thermocouple as described in Chapter IV. Two separate units were tested under the same conditions.

The initial sharp decrease in resistance in Figure 5 at room temperature is due to the rectifying contacts on the silicon heater as discussed in Chapter III. Once the rectifying contact breaks down, the extrinsic curve for both heaters takes on the shape comparable to the extrinsic region in Figure 4, page 20.

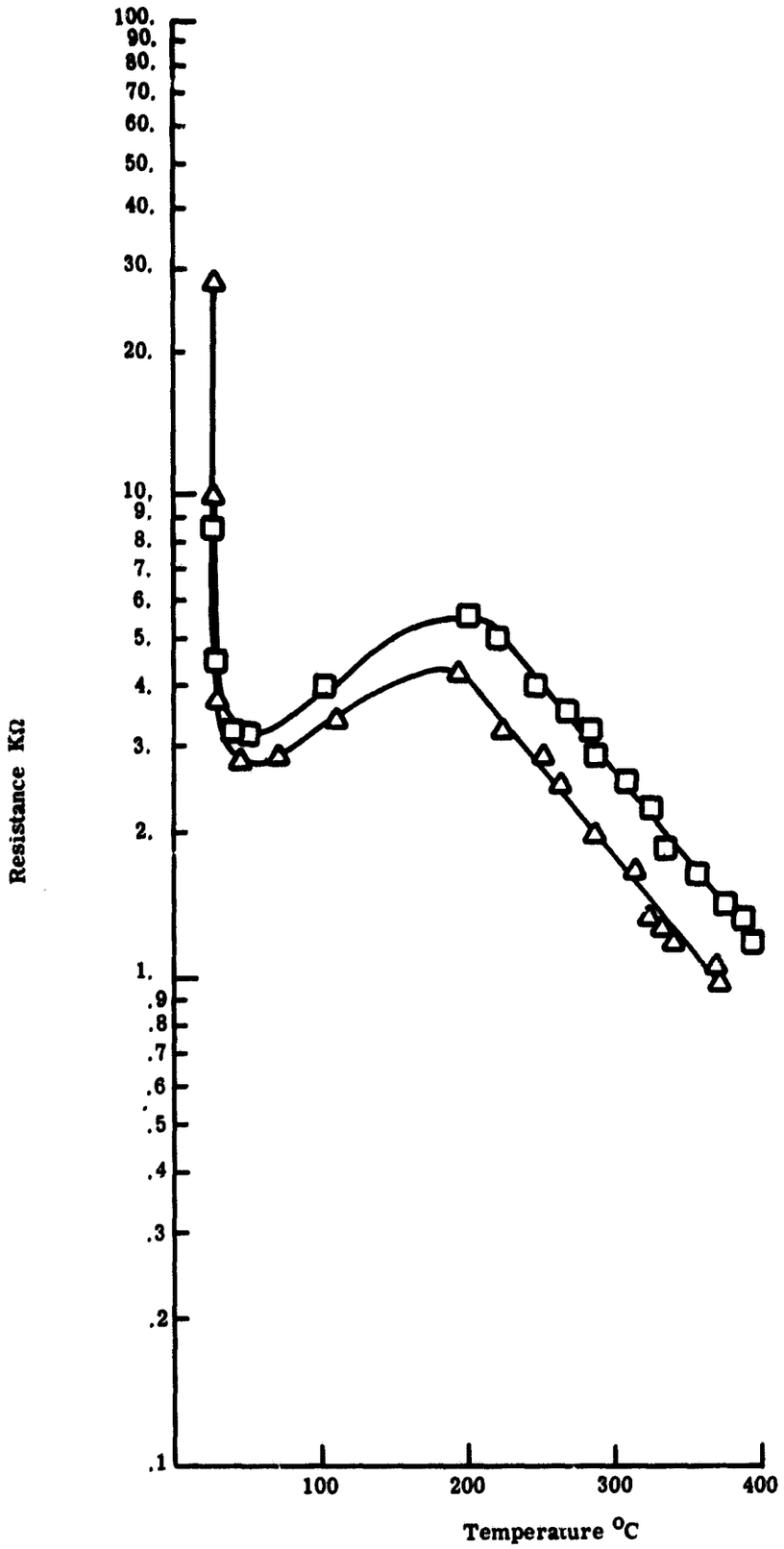

Figure 5.- Experimental resistance - temperature characteristics for silicon bar.

The transfer from extrinsic conduction occurs at approximately 200° C, which is the theoretical value for silicon (Ref. 7, p. 209).

The intrinsic curve for both heaters is a straight line with a negative slope. This is comparable to the similar region of Figure 4, page 20. The slopes of the two curves are approximately the same, but one heater bar has a higher resistance than the other. This is most likely due to physical differences between the two heaters. The silicon bars were cut from a 0.016-inch-thick wafer and then chemically etched down to a nominal 0.010-inch-square cross section. A 20 per cent difference in the cross-sectional dimension would be sufficient to cause this difference in resistance. When the possible variation in length and cross-sectional dimensions are considered, these differences are reasonable.

Equation (12) shows that the slope of a curve of $\ln \rho$ versus $1/T$ in the intrinsic region should be equal to $E_g/2k$. The dashed line in Figure 6 is a representative slope that a sample of silicon with an energy gap equal to 1.1 electron volts should exhibit. The two plotted curves are the experimental data from Figure 5, page 26, plotted against reciprocal temperature. The theoretical slope is

$$\text{Slope}_{\text{theoretical}} = \frac{1.1}{(2)(8.617 \times 10^{-5})} = 6.38 \times 10^{3}$$

The slope of the experimental data is

$$\text{Slope}_{\text{experimental}} = \frac{(\ln 10^{4} - \ln 1.2 \times 10^{3})}{(2.18 \times 10^{-3} - 1.5 \times 10^{-3})} = 3.11 \times 10^{3}$$

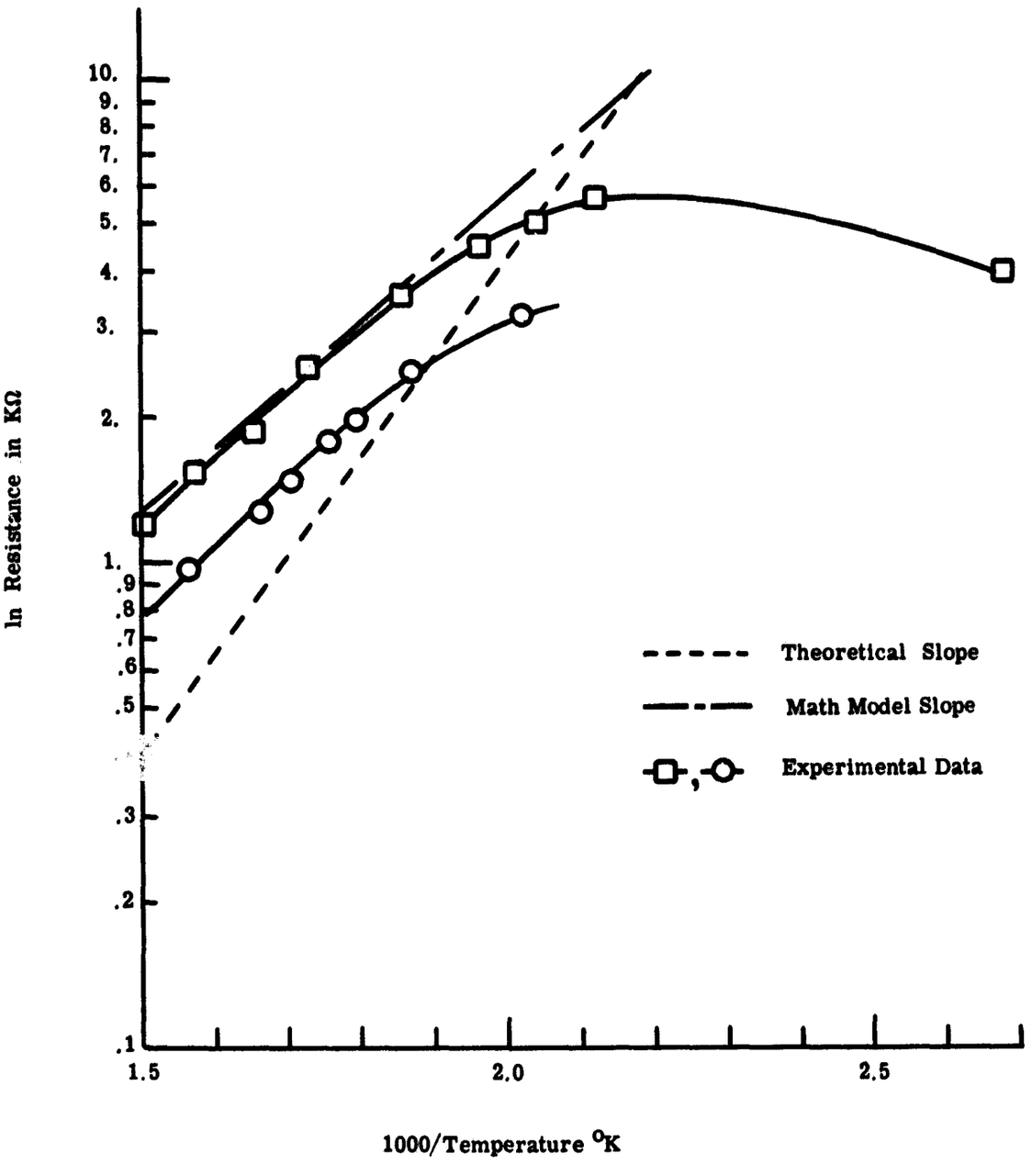

Figure 6.- Comparison of the slopes of the log resistance vs reciprocal temperature for the theoretical, mathematical model, and experimental data.

This difference in slope is due to the fact that in the experimental case the heater bar is not all at the same temperature. The experimental curve is for the average resistance for the whole heater plotted against the maximum temperature.

The mathematical model developed in Chapter VI was used to calculate the temperature distribution along the heater for three different maximum temperatures. Using the theoretical variation of resistivity with temperature for the intrinsic region and two straight line approximations of the data in Figure 2, page 10, for the extrinsic region, the average resistivity of the bar was calculated. The slope of the mathematical model data plotted in Figure 6, page 28, is slightly smaller than that of the experimental data. The mathematical model slope is

$$\text{Slope}_{\text{model}} = 3.0 \times 10^3$$

This is only 3.6 per cent smaller than the experimental slope. This is sufficiently close to verify that the slope of the experimental data is due to the temperature distribution along the heater.

CHAPTER VI

TEMPERATURE DISTRIBUTION ON THE HEATER

As discussed in the last chapter, the temperature distribution on the heater bar has a significant effect on its operation. The temperature distribution will be discussed on the basis of a mathematic model and experimental data.

The following assumptions have been made for this model:

1. No temperature variation through heater cross section.
2. Heater is symmetrical about its center.
3. Maximum temperature exists at the center.
4. To avoid trial and error solution, the boundary conditions will be taken from the experimental data.
5. Heat flow into a volume element is positive.

The heat balance equation for any volume element in the heater consists of

$$q_1 + q_2 + q_g + q_r + q_c = 0 \qquad (13)$$

where

q_1 = rate of conductive heat flow into the volume element in Btu/hr

q_2 = rate of conductive heat flow out of the volume element in Btu/hr

q_g = rate of heat generation inside the volume element in Btu/hr

q_r = rate of radiant heat loss from the surface in Btu/hr

q_c = rate of free convective heat loss from the surface in Btu/hr

$$q_1 = -kA \left.\frac{dT}{dx}\right|_x$$

$$q_2 = +kA \left.\frac{dT}{dx}\right|_{x+\Delta x} = kA \left.\frac{dT}{dx}\right|_x + kA \left.\frac{d^2T}{dx^2}\right|_x \tag{14}$$

$$q_g = 3.41I^2R = 3.41I^2\rho \frac{dx}{D^2} \tag{15}$$

From equation (2),

$$q_r = 4Dh_r(T - T_o)dx \tag{16}$$

From equation (1),

$$q_c = -4Dh_c(T - T_o)dx \tag{17}$$

Combining equations (13), (14), (15), (16), and (17) gives

$$kA \frac{d^2T}{dx^2} + \frac{3.41I^2\rho}{A} - 4D(h_r + h_c)(T - T_o) = 0 \tag{18}$$

The quantities k, ρ, h_r, and h_c are all temperature dependent so equation (18) is a nonlinear differential equation. The most practical solution for this equation is a numerical solution with the following approximations for the temperature dependent factors:

For $T > 300^{\circ}$ C

$$\rho_{ohm\text{-}ft} = 2.49 \times 10^{-6}\, e^{6.38\times10^{3}/(T+273)}$$

For 200° C $< T < 300^{\circ}$ C

$$\rho_{ohm\text{-}ft} = 0.383\, e^{-2.60\times10^{-3}T}$$

For $T < 200^{\circ}$ C

$$\rho_{ohm\text{-}ft} = 0.0754\, e^{5.58\times10^{-3}T}$$

The approximation for $T > 300^{\circ}$ C is from the intrinsic curve of Figure 2, page 10, and the other two are from the extrinsic curve in Figure 4, page 20.

$$k_{Btu/hr\text{-}ft\text{-}^{\circ}F} = 3.38 \times 10^{3}\ T^{-0.57}$$

(Ref. 8, p. 99)

From equation (2)

$$h_r = \alpha F_t$$

where

$\alpha = 0.72$ (Ref. 9, p. 70)

$$h_c = 0.234\left[\frac{(T - T_o)}{D}\right]^{1/4}$$ (Ref. 5, p. 314)

The computer program and the data readout for the numerical solution for the mathematical model are given in the appendix. Figure 7 is a plot of the mathematical model and experimental temperature distribution. The experimental distribution agrees reasonably well with the model distribution for the middle region of the bar. The end region temperatures are of little importance for the operation of the sensor since in order to keep the temperature variation along the zinc oxide film within approximately 50° C, the film would be deposited only within 0.050 inch of the center. Within this region the model is sufficiently accurate to predict the temperature distribution.

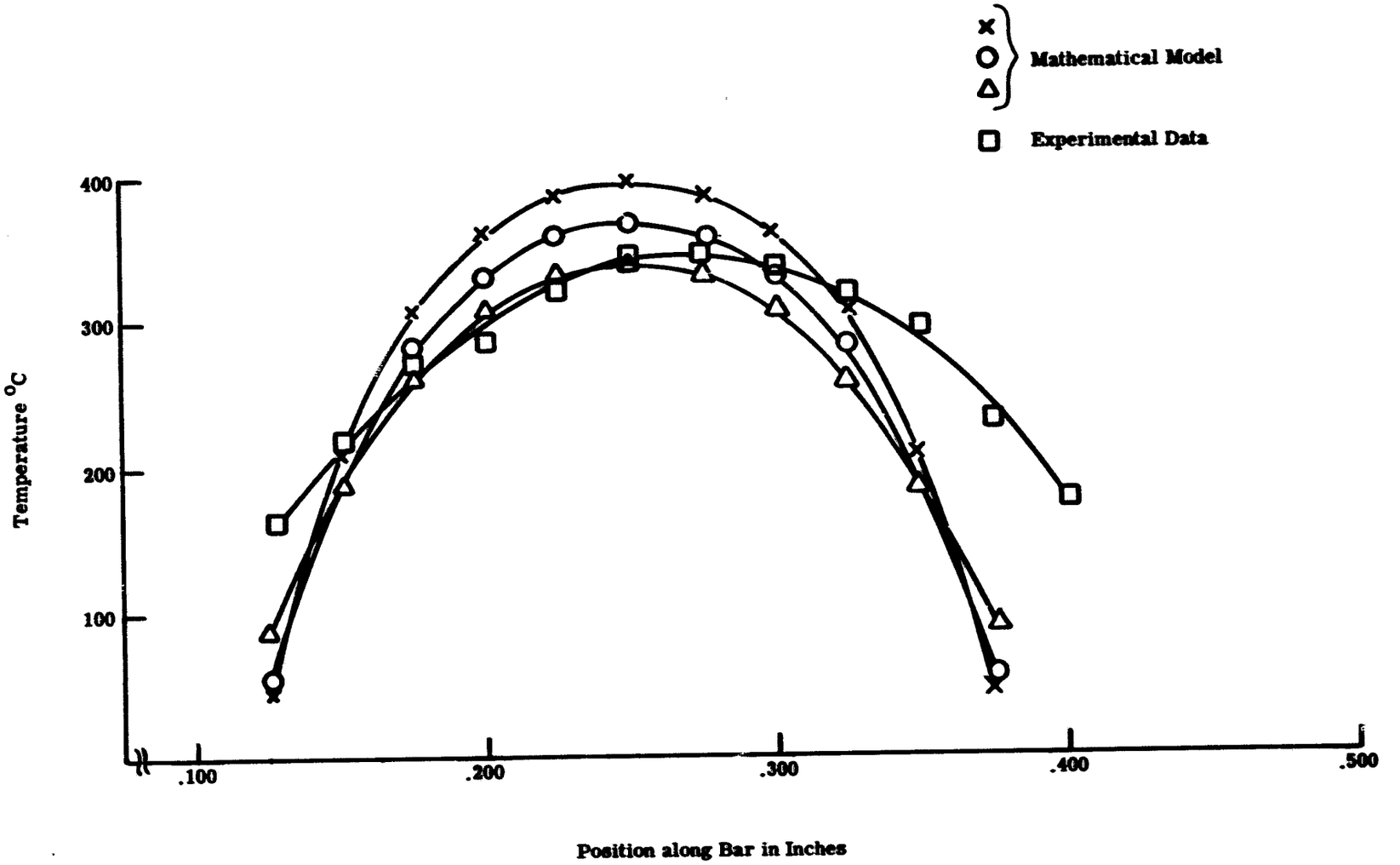

Figure 7.- Temperature distribution along heater.

CHAPTER VII

POWER REQUIREMENTS OF HEATER

Because of its small size, the heater can be operated in a completely uninsulated condition. Since silicon has a negative temperature coefficient of resistance in the intrinsic state, the heater must be operated from a constant current power supply. If operated from a constant voltage supply, a completely unstable condition will result at temperatures about 200° C and the temperature will increase quickly to the melting point for silicon.

Figure 8 shows the current and corresponding voltage required as a function of the maximum heater temperature for a typical heater. A 50-milliamp constant current power supply capable of putting out 100 volts would be required to power the heater with no forced convection and no insulation.

Figure 9 shows the power required to heat the heater in the uninsulated condition as a function of maximum temperature. The heater required approximately 2.5 watts of power to reach a maximum temperature of 400° C.

In a final configuration this power requirement should be able to be reduced through the use of a reflecting radiation shield around the heater.

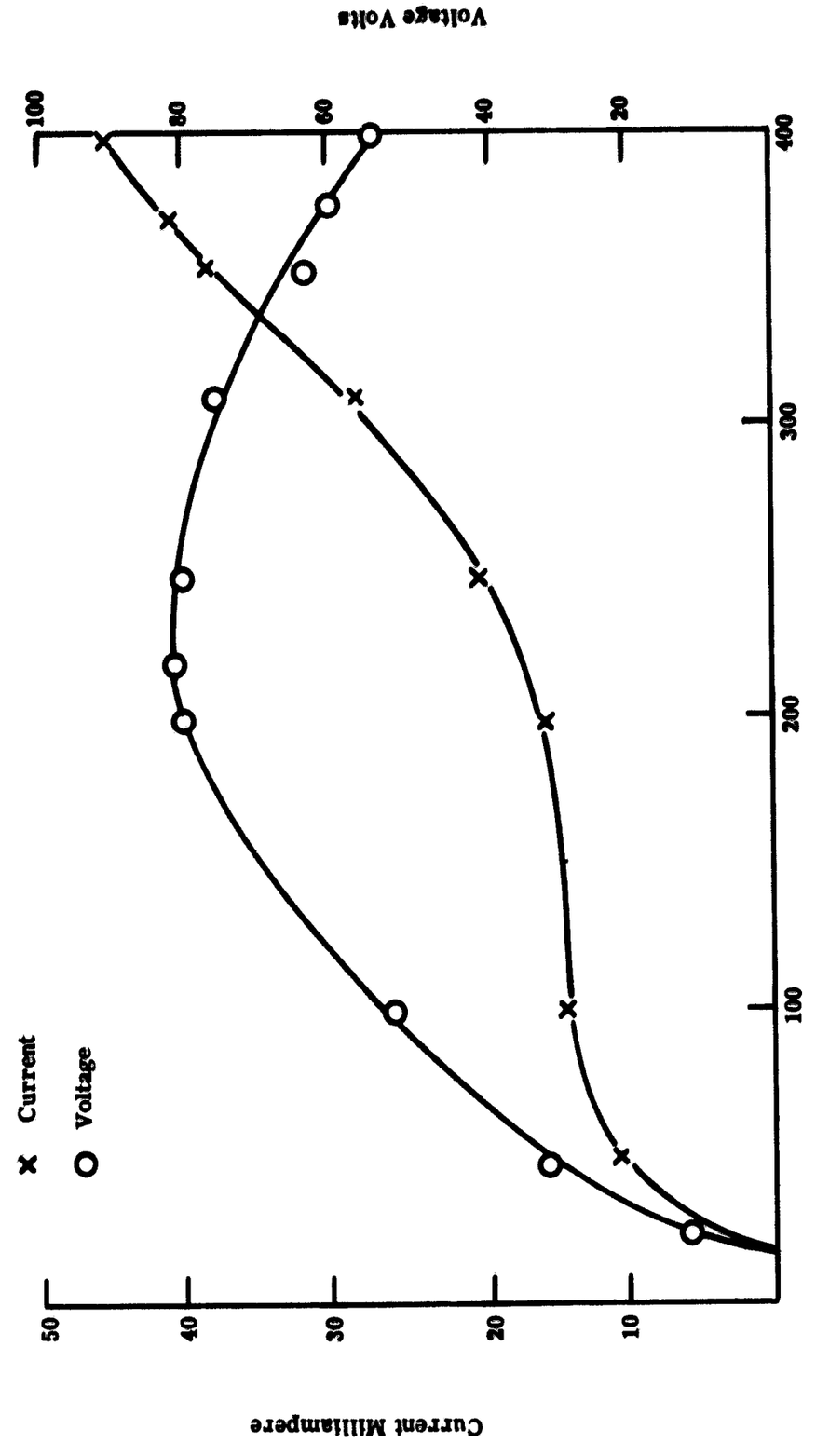

Figure 8.- Current-voltage requirements of the heater.

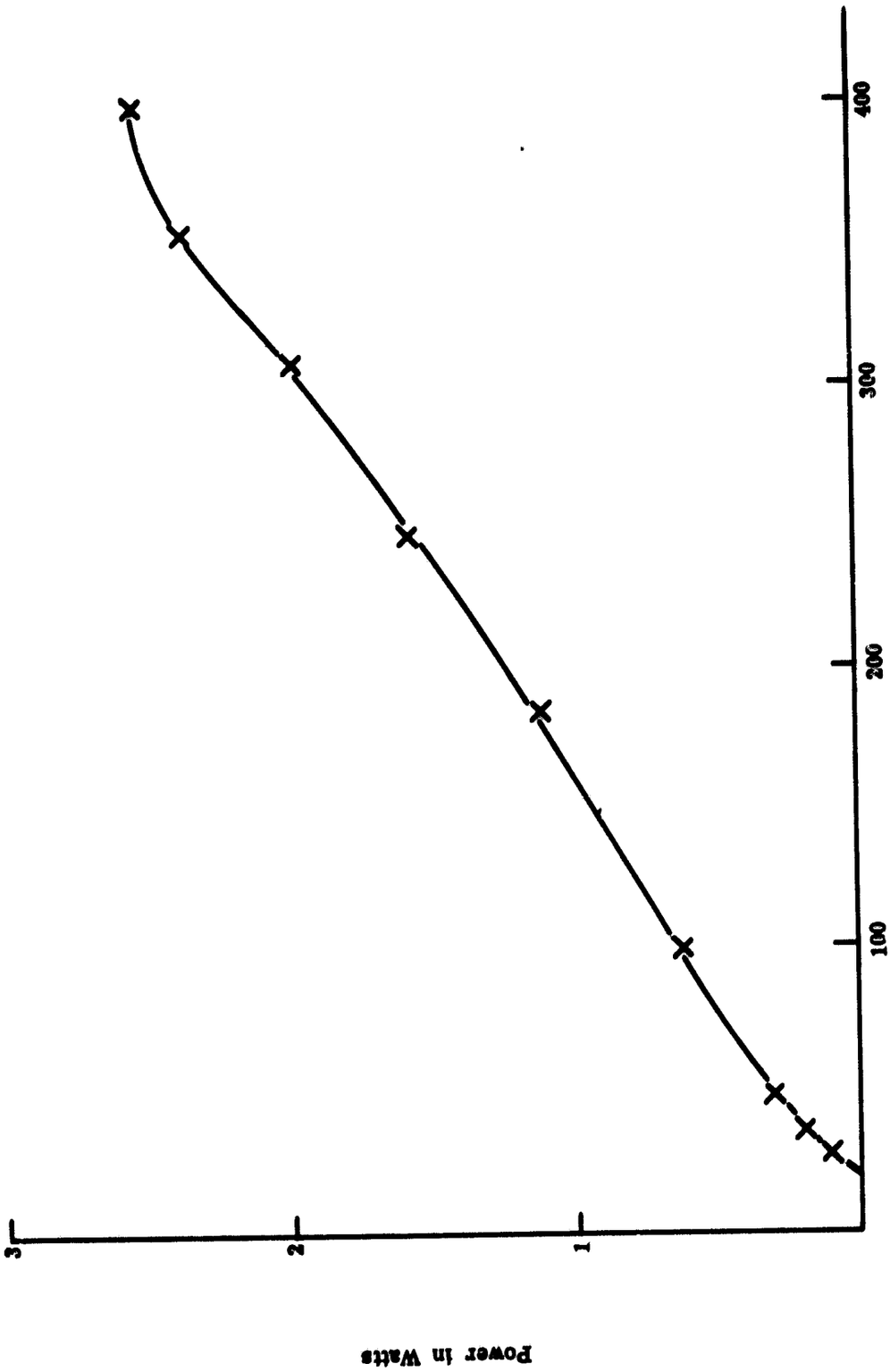

Figure 9.- Power requirements of heater.

CHAPTER VIII

CONCLUSIONS

This work has shown that the use of a small-diameter heater for a zinc oxide oxygen sensor is feasible and will result in a considerable reduction in size and power requirements.

The temperature of the heater can be sensed by measuring its average resistance. A significant variation in the resistance characteristics for different elements has been noted, but the slope of the log resistance versus temperature curve for the operating temperature region is repeatable between different heaters. Also, the maximum voltage occurs at approximately the start of the intrinsic region at 200° C. Thus, if the current is increased from the point of maximum voltage until the logarithm of the resistance has decreased by the slope of the experimental data divided by the temperature change, an approximate operating point can be determined.

Thus, from the data of Figure 5, page 26,

$$\ln R = K - 8.12 \times 10^{-3} T\ (^{\circ}C)$$

$$\Delta \ln R = \Delta(-8.12 \times 10^{-3} T)$$

$$R_2 = R_1\, e^{-8.12 \times 10^{-3}(T_2 - T_1)}$$

so that

$$R_{400^{\circ} C} = 0.197\, R_{200^{\circ} C} \qquad (19)$$

Using the two values of $R_{200^\circ C}$ from Figure 5, page 26, of 5.7 K and 4.1 K, $R_{400^\circ C}$ calculated from equation (19) is 1.12 K and 0.81 K, respectively. These values would give a temperature error of about 10° C.

This effort has shown mainly that this type of heater is feasible, but considerably more work needs to be accomplished before a prototype sensor can be built. The techniques of electrically isolating the zinc oxide film from the heater and depositing the film on the surface still have to be worked out.

REFERENCES

1. Heiland, G.; Mollwo, E.; Stöckman, F.: "Electronic Processes in Zinc Oxide." Solid State Physics, vol. 8, Academic Press, New York, 1959.

2. Beven, D. J. M.; Anderson, J. S.: Discussions Faraday Society. 8:238, 1950, cited by Ref. 1, p. 249.

3. Kefeli, A.: Diplomarbeit. University of Erlanger, 1957, cited by Ref. 1, p. 277.

4. Royal, T. M.; Wortman, J. J.; Monteith, L. K.: "An Investigation of Thin Film Oxygen Partial Pressure Sensors." NASA CR 1182, 1968.

5. Kreith, F.: Principles of Heat Transfer. International Textbook Company, Scranton, 1958.

6. Integrated Silicon Device Technology Volume I - Resistance. USAF ASD-TDR-63-316, 1963.

7. Azaroff, L. V.; Brophy, J. J.: Electronic Processes in Materials. McGraw-Hill Book Company, New York, 1963.

8. Integrated Silicon Device Technology Volume V. USAF ASD-TDR-63-316, 1963.

9. International Journal of Heat and Mass Transfer Volume 5. Pergamon Press, New York, 1962.

```
JOB NO. 1302 ASSIGNED TO  JOB,1,100,40000.          A1965       2,CARL R PEARSON   T

START OF OUTPUT FOR JOB NO. 1302.
        TER1302.
        JOB,1,100,40000.          A1965       2,CARL R PEARSON   T8C125,1202

              PROGRAM TEMP(INPUT,OUTPUT)
000003        DIMENSION Y(200),T(200),X(200)
000003        TAMB=75.
000004        T(1)=743.
000006        DX=4.16E-04
000007        AR=5.95E-07
000011        D=8.34E-04
000012        CI=.045
000014        DO3001=1,3
000016        RHOT=0.
000017        Y(1)=0.
000017        X(1)=0.
000020        TC=(T(1)-32.)*5./9.
000024        PRINT2,TAMB,T(1),TC,X(1)
000040      2 FORMAT(//13X,12HTEMP. DEG. F,6X,12HTEMP. DEG. C,5X,15HPOSITION INC
             1HES,5X,9HTAMBIENT=F10.3/14X,F10.3,8X,F10.3,9X,F10.3)
000040        N1=41
000041        DO100N=2,N1
000043        X(N)=X(N-1)+DX*12.
000046        A=T(N-1)
000047        B=A-TAMB
000051        HR=.72*.172*(((A+460.)/100.)**4-819.25)/B
000060        HC=.27*(B/D)**.25
000065        TK=3.38E03/A**.57
000071        IF(A-572.)10,10,30
000074       10 IF(A-392.)11,11,12
000077       11 RHO=.0754*EXP(5.58E-03*5.*(A-32.)/9.)
000107          GO TO 40
000107       12 RHO=.383*EXP(-2.60E-03*5.*(A-32.)/9.)
000117          GO TO 40
000117       30 RHO=2.49E-06*EXP(6.38E03/((A-32.)*5./9.+273.))
000130       40 RHOT=RHOT+RHO
000132          SLY=(4.*D*(HR+HC)*B-3.41*CI**2*RHO/AR)/(TK*AR)
000146          Y(N)=Y(N-1)+SLY*DX
000152          T(N)=T(N-1)+Y(N)*DX
000155          IF(T(N).LE.TAMB)N1=N
000161          TC=(T(N)-32.)*5./9.
000165      100 PRINT1,T(N),TC,X(N),RHOT
000204        1 FORMAT(14X,F10.3,8X,F10.3,9X,F10.3,9X,F10.3)
000204      200 T(1)=T(1)-50.
000206      300 CI=CI-.008
000212          STOP
```

```
000214          END

PROGRAM LENGTH INCLUDING I/O BUFFERS
005551
FUNCTION ASSIGNMENTS
STATEMENT ASSIGNMENTS
1       -  000300     2       -  000236     10      -  000074     11      -  000077
12      -  000107     30      -  000117     40      -  000130     200     -  000204
BLOCK NAMES AND LENGTHS
VARIABLE ASSIGNMENTS
A       -  001476     AR      -  001466     B       -  001477     CI      -  001470
D       -  001467     DX      -  001465     HC      -  001501     HR      -  001500
I       -  001471     N       -  001475     N1      -  001474     RHO     -  001503
RHOT    -  001472     SLY     -  001504     T       -  000600     TAMB    -  001464
TC      -  001473     TK      -  001502     X       -  001154     Y       -  000334
START OF CONSTANTS
000216
START OF TEMPORARIES
000310
START OF INDIRECTS
000325
UNUSED COMPILER SPACE
002100
```

TEMP. DEG. F	TEMP. DEG. C	POSITION INCHES	TAMBIENT= 7.500E+01
7.430E+02	3.950E+02	0.	
7.420E+02	3.944E+02	4.992E-03	3.500E-02
7.399E+02	3.933E+02	9.984E-03	7.029E-02
7.368E+02	3.916E+02	1.498E-02	1.062E-01
7.326E+02	3.892E+02	1.997E-02	1.420E-01
7.273E+02	3.863E+02	2.496E-02	1.910E-01
7.208E+02	3.827E+02	2.995E-02	2.207E-01
7.132E+02	3.784E+02	3.494E-02	2.626E-01
7.042E+02	3.734E+02	3.993E-02	3.072E-01
6.938E+02	3.676E+02	4.493E-02	3.554E-01
6.818E+02	3.610E+02	4.992E-02	4.080E-01
6.682E+02	3.534E+02	5.491E-02	4.664E-01
6.527E+02	3.448E+02	5.990E-02	5.324E-01
6.340E+02	3.350E+02	6.490E-02	6.084E-01
6.147E+02	3.237E+02	6.989E-02	6.983E-01
5.914E+02	3.108E+02	7.488E-02	8.078E-01
5.643E+02	2.957E+02	7.987E-02	9.467E-01
5.324E+02	2.780E+02	8.486E-02	1.124E+00
4.956E+02	2.576E+02	8.986E-02	1.310E+00
4.540E+02	2.344E+02	9.485E-02	1.500E+00
4.074E+02	2.086E+02	9.984E-02	1.714E+00
3.558E+02	1.799E+02	1.048E-01	1.937E+00
3.000E+02	1.480E+02	1.098E-01	2.143E+00
2.409E+02	1.161E+02	1.148E-01	2.316E+00
1.794E+02	8.189E+01	1.198E-01	2.460E+00

1.162E+02	4.679E+01	1.248E-01	2.579E+00
5.198E+01	1.110E+01	1.298E-01	2.677E+00

TEMP. DEG. F	TEMP. DEG. C	POSITION INCHES	TAMBIENT= 7.500E+01
6.930E+02	3.672E+02	0.	
6.920E+02	3.667E+02	4.992E-03	5.297E-02
6.899E+02	3.655E+02	9.984E-03	1.064E-01
6.868E+02	3.638E+02	1.498E-02	1.608E-01
6.827E+02	3.615E+02	1.997E-02	2.167E-01
6.774E+02	3.585E+02	2.496E-02	2.747E-01
6.709E+02	3.550E+02	2.995E-02	3.354E-01
6.632E+02	3.507E+02	3.494E-02	3.998E-01
6.542E+02	3.457E+02	3.994E-02	4.688E-01
6.438E+02	3.399E+02	4.493E-02	5.437E-01
6.318E+02	3.332E+02	4.992E-02	6.263E-01
6.180E+02	3.256E+02	5.491E-02	7.190E-01
6.023E+02	3.168E+02	5.990E-02	8.249E-01
5.842E+02	3.068E+02	6.490E-02	9.401E-01
5.634E+02	2.952E+02	6.989E-02	1.099E+00
5.394E+02	2.819E+02	7.488E-02	1.276E+00
5.122E+02	2.668E+02	7.987E-02	1.461E+00
4.816E+02	2.498E+02	8.486E-02	1.652E+00
4.478E+02	2.310E+02	8.986E-02	1.852E+00
4.106E+02	2.103E+02	9.485E-02	2.062E+00
3.700E+02	1.878E+02	9.984E-02	2.284E+00
3.264E+02	1.635E+02	1.048E-01	2.499E+00
2.802E+02	1.379E+02	1.098E-01	2.687E+00
2.321E+02	1.111E+02	1.148E-01	2.849E+00
1.824E+02	8.355E+01	1.198E-01	2.989E+00
1.316E+02	5.531E+01	1.248E-01	3.110E+00
7.990E+01	2.661E+01	1.298E-01	3.212E+00
2.772E+01	-2.376E+00	1.348E-01	3.300E+00

TEMP. DEG. F	TEMP. DEG. C	POSITION INCHES	TAMBIENT= 7.500E+01
6.430E+02	3.394E+02	0.	
6.421E+02	3.389E+02	4.992E-03	8.325E-02
6.401E+02	3.379E+02	9.984E-03	1.672E-01
6.373E+02	3.363E+02	1.498E-02	2.528E-01
6.334E+02	3.341E+02	1.997E-02	3.407E-01
6.285E+02	3.314E+02	2.496E-02	4.319E-01
6.225E+02	3.280E+02	2.995E-02	5.276E-01
6.153E+02	3.241E+02	3.494E-02	6.291E-01
6.069E+02	3.194E+02	3.994E-02	7.379E-01
5.972E+02	3.140E+02	4.493E-02	8.564E-01
5.860E+02	3.078E+02	4.992E-02	9.872E-01
5.731E+02	3.006E+02	5.491E-02	1.134E+00
5.584E+02	2.925E+02	5.990E-02	1.303E+00
5.418E+02	2.832E+02	6.490E-02	1.482E+00
5.231E+02	2.729E+02	6.989E-02	1.665E+00

5.025E+02	2.614E+02	7.488E-02	1.853E+00
4.799E+02	2.488E+02	7.987E-02	2.048E+00
4.552E+02	2.351E+02	8.486E-02	2.248E+00
4.285E+02	2.203E+02	8.986E-02	2.450E+00
3.997E+02	2.043E+02	9.485E-02	2.672E+00
3.689E+02	1.872E+02	9.984E-02	2.907E+00
3.362E+02	1.690E+02	1.048E-01	3.111E+00
3.011E+02	1.499E+02	1.098E-01	3.305E+00
2.662E+02	1.301E+02	1.148E-01	3.470E+00
2.294E+02	1.097E+02	1.198E-01	3.635E+00
1.917E+02	8.973E+01	1.248E-01	3.774E+00
1.532E+02	6.735E+01	1.298E-01	3.890E+00
1.142E+02	4.565E+01	1.348E-01	4.007E+00
7.466E+01	2.370E+01	1.398E-01	4.105E+00 -

```
06/13/69   LRC CM SCOPE 3.0  6600C-131K 04/16/69
10.26.28.TER1302.
10.26.28.JOB,1,100,40000.          A1965       2,
10.26.28.CARL R PEARSON   T0C125,1202
10.26.29.NOMAP.
10.26.29.RUN(S)
10.26.33.LGO.
10.26.35.MEMORY  011400 CM
10.26.36.STOP
10.26.36.CPU      0.502452 SEC.
10.26.36.PPU      9.515008 SEC.
10.26.36.DATE      06/13/69

END OF OUTPUT FOR JOB NO. 1302.

JOB NO. 1302 IS COMPLETE.
```